2-21-2024

Simulation of the Multi-Wake Evolution of Two Sandia National Labs/National Rotor Testbed Turbines Operating in a Tandem Layout

Apurva Baruah
Michigan Technological University, baruah@mtu.edu

Fernando L. Ponta
Michigan Technological University, flponta@mtu.edu

Alayna Farrell
Michigan Technological University, anfarrel@mtu.edu

Recommended Citation

Baruah, A., Ponta, F. L., & Farrell, A. (2024). Simulation of the Multi-Wake Evolution of Two Sandia National Labs/National Rotor Testbed Turbines Operating in a Tandem Layout. *Energies, 17*(5). http://doi.org/10.3390/en17051000
Retrieved from: https://digitalcommons.mtu.edu/michigantech-p2/589

Follow this and additional works at: https://digitalcommons.mtu.edu/michigantech-p2

 Part of the Mechanical Engineering Commons

energies

MDPI

Article

Simulation of the Multi-Wake Evolution of Two Sandia National Labs/National Rotor Testbed Turbines Operating in a Tandem Layout

Apurva Baruah, Fernando Ponta * and Alayna Farrell

Department of Mechanical Engineering-Engineering Mechanics, Michigan Technological University, Houghton, MI 49931, USA; baruah@mtu.edu (A.B.); anfarrel@mtu.edu (A.F.)
* Correspondence: flponta@mtu.edu

Abstract: The future of wind power systems deployment is in the form of wind farms comprised of scores of such large turbines, most likely at offshore locations. Individual turbines have grown in span from a few tens of meters to today's large turbines with rotor diameters that dwarf even the largest commercial aircraft. These massive dynamical systems present unique challenges at scales unparalleled in prior applications of wind science research. Fundamental to this effort is the understanding of the wind turbine wake and its evolution. Furthermore, the optimization of the entire wind farm depends on the evolution of the wakes of different turbines and their interactions within the wind farm. In this article, we use the capabilities of the Common ODE Framework (CODEF) model for the analysis of the effects of wake–rotor and wake-to-wake interactions between two turbines situated in a tandem layout fully and partially aligned with the incoming wind. These experiments were conducted in the context of a research project supported by the National Rotor Testbed (NRT) program of Sandia National Labs (SNL). Results are presented for a layout which emulates the turbine interspace and relative turbine emplacement found at SNL's Scaled Wind Technologies Facility (SWiFT), located in Lubbock, Texas. The evolution of the twin-wake interaction generates a very rich series of secondary transitions in the vortex structure of the combined wake. These ultimately affect the wake's axial velocity patterns, altering the position, number, intensity, and shape of localized velocity-deficit zones in the wake's cross-section. This complex distribution of axial velocity patterns has the capacity to substantially affect the power output, peak loads, fatigue damage, and aeroelastic stability of turbines located in subsequent rows downstream on the farm.

Keywords: vortex lattice methods; wind farm simulation; wind turbine wake; vortex dynamics; wake analyses; wind farm array; wind farm layout

Citation: Baruah, A.; Ponta, F.; Farrell, A. Simulation of the Multi-Wake Evolution of Two Sandia National Labs/National Rotor Testbed Turbines Operating in a Tandem Layout. *Energies* **2024**, *17*, 1000. https://doi.org/10.3390/en17051000

Academic Editor: Christopher Jung

Received: 8 January 2024
Revised: 9 February 2024
Accepted: 18 February 2024
Published: 21 February 2024

1. Introduction

Decades of research and development have led to the continuous deployment of commercial wind power systems. Individual turbines have grown in span from a few tens of meters to today's large turbines with rotor diameters that dwarf even the largest commercial aircraft. The future of wind power systems deployment is in the form of wind farms comprised of scores of such large turbines, most likely at offshore locations. These massive dynamical systems present unique challenges at scales unparalleled in prior applications of wind science research. As reported by Dykes et al. [1], Veers et al. [2], and Meneveau [3], a deeper understanding of the complex phenomena associated with the wind turbine wake and the prediction of power and loads of turbines in waked conditions is indispensable. The successful design, development, deployment, operation, and optimization of the upcoming generation of wind power systems requires a holistic understanding of all the multi-physics phenomena at their respective temporal and physical scales, with the overarching goal of maximizing power production while keeping costs low.

Fundamental to this effort is the understanding of the wind turbine wake and its evolution. Furthermore, the optimization of the entire wind farm depends on the evolution of the wakes of different turbines and their interactions within the wind farm. Turbines operating in the wakes of others can experience power losses upto 40% on an individual basis and up to 25% for the entire wind farm, which has obvious economic consequences.

Another consequence of the wakes is the higher dynamical loads experienced by the waked rotors. These higher dynamical loads are primarily caused by two reasons. Firstly, the wake's inherent turbulence compounds the turbulence of the existing atmospheric boundary layer, thereby intensifying the overall turbulence in the wake as compared to the undisturbed wind. Secondly, turbulent fluctuations within the atmospheric boundary layer in the lateral and vertical directions lead to *wake meandering*. This meandering wake leads to intermittent interactions between the wake and the downwind rotors, which significantly increases the loads it experiences. And although wake-induced loading is addressed in the IEC design standards for wind turbines [4], these approximations therein do not completely account for the complex, dynamic wake evolution and interactions.

The decrease in the power generated by wake rotors results in the direct loss of revenue and an increase in the cost of energy. The uncertainties of the wake-induced fatigue loads leads to a decrease in the rotor reliability and increases operational and maintenance expenses, which in turn increases the the cost of energy. These costs scale significantly for offshore installations with their inherently higher infrastructure and logistical costs. Hence, there is a huge incentive for the study and analysis of wind turbine wakes and their turbine-to-turbine interactions.

Wind tunnel experiments offer comparable controlled and reproducible flow conditions. However, typically only a few physical features of the actual operation of wind turbines can be simulated in wind tunnel experiments. A thorough study of wakes in wind farms is practically impossible because of the extremely high difference in scale between an eventual wind-tunnel model and the actual size of a wind farm, plus the impossibility of reproducing in detail the transient and spatially varying nature of wind in a controlled manner. Hence, computational models and simulations are indispensable tools available for improving our understanding of the wakes and their evolution and interaction through the wind farm.

To this end, several computational flow models have been developed ranging from simplified, analytical models [5] to CFD techniques, like Reynolds-Averaged Navier–Stokes (RANS) [6–8], Large Eddy Simulation (LES) [9–13], and Direct Numerical Simulation (DNS) [14]. Depending on the target applications, these different models have varying accuracy and costs [15,16].

Additionally, these flow models need to be integrated with structural models to capture the dynamics of the turbine blades/rotors. The structural response of the rotors can be studied using reduced order models and modal analysis, leading up to complex, full 3D finite elements. The most successful reduced-order models for the aeroelastic study of the turbines belong to the Blade Element Momentum (BEM) family (see Manwell et al. [17] and Burton et al. [18], among others). These models differ in their underlying assumptions and implementations, which lead to different results based on each modeler or code. These differences can amount to an unquantified level of uncertainty for decisions of the control systems of any of the individual turbines located downstream and of the collective control system of the wind farm as a whole.

Hence, there is a need for modeling systems that successfully integrate the different coupled, multi-scale physics of wind generation systems. Such a comprehensive modeling system needs to have the capabilities to solve all the non-linear, coupled physical phenomena associated with the entire wind farm at their appropriate temporal and spatial scales. The results and solutions from such a system should be obtained at appropriate fidelity using reasonable computational resources.

In this article, we use the capabilities of the Common ODE Framework (CODEF) model, introduced in Ponta et al. [19], for the analysis of the effects of wake–rotor and

wake-to-wake interactions between two turbines situated in a tandem layout fully and partially aligned with the incoming wind. These experiments were conducted in the context of a research project supported by the National Rotor Testbed (NRT) program of Sandia National Labs (SNL). Results are presented for a layout which emulates the turbine interspace and relative turbine emplacement found at SNL's Scaled Wind Technologies Facility (SWiFT), located in Lubbock, Texas.

The CODEF multi-physics suite involves the successful coupling of the aero-elasto-intertial physics of an individual turbine with the overall farm flow, including the evolution and interaction of the wakes of multiple turbines on the wind farm. With our modeling system, other aspects of the wind farm dynamics, like the farm-collective control strategies involving the different electro-mechanical components, the farm microgrid, and ultimately the overall grid dynamics, can also be included. This *unified* modeling paradigm enables the study of the turbine-to-turbine interaction in the twin-wake evolution and the accurate representation of the loads on the waked rotors. Before we discuss the series of numerical experiments on the twin-turbine layout, we shall present a brief description of CODEF in the following section.

2. The Common ODE Framework (CODEF)

As a multiphysics modeling suite for wind turbine operation, the Common ODE Framework (CODEF) evaluates multivariable ODE solutions in time to simulate aspects of wind turbine and collective farm dynamics. Interactive modules within the framework are designed to model components such as blade structure, electromechanical devices, controls systems, and fluid flow at an individual and multi-turbine scale. These CODEF modules are inter-dependent subroutines that define characteristic boundary conditions and governing equations to guide the non-linear, variable-order solution of the central ODE system. Solutions are resolved at variable time-steps by integrating all system modules in unison with regulation of local truncation error, which acts to stabilize and efficiently pace the iteration of evaluations. For additional discussions of CODEF modules, structure, and validation studies, see Ponta et al. [19].

As a modular structure, CODEF can be customized to model expanded dynamics of wind turbine and farm operation. Recently, more robust modules for farm-collective controls, intra-farm microgrid electrical components, and farm-flow interactions have been developed for CODEF integration via implementations of the Gaussian-Core Vortex-Lattice Model (GVLM) described in Section 2.3. Using simulations performed with these recent additions to CODEF, this work will highlight how changes to the flexibility of turbine blades affect the aeroelastic dynamics of turbine operation and associated farm-flow interactions.

2.1. Blade Structure Model

As a wind turbine operates, the blade's shape and attitude change substantially in response to fluctuating aerodynamic forces from oncoming wind. To produce a high-fidelity representation of a warping blade structure at an economical computational expense, CODEF implements the Generalized Timoshenko Beam Model (GTBM), introduced in Hodges et al. [20,21]. This model uses a reduction-of-order technique to transform the 3D computation of blade structural deformation into a 1D nonlinear analysis of pre-evaluated 2D finite-element solutions along the blade's span [19].

Similar to the classic Timoshenko beam model, the GTBM represents the blade as a beam with equivalent stiffness but withdraws the original model's assumption that blade section profiles must remain planar. Thus, at each time-step of the ODE solution, instantaneous warping of a blade section is interpolated from the pre-solved 2D finite-element evaluations along the blade's span. Three-dimensional representation of strain energy can then be solved in terms of 1D variables from the classic Timoshenko model to provide an accurate representation of the blade using a 6×6 stiffness matrix which includes all coupled modes of deformation [22].

Solutions of blade structure at time iterations of the ODE solution are imperative to the overall simulation of turbine operation. The structural model interacts closely with the CODEF models of rotor flow and vortex structure to evaluate the dynamics of blade aeroelastic behavior and turbine vortex-wake interactions. Without knowing the instantaneous warping of blade sections, we would not be able to properly evaluate the dynamic deformation of the rotor or how these deformations would affect vortex generation in the wake.

2.2. Rotor Flow Model

The CODEF model for rotor flow was developed by adapting a classical Blade Element Momentum (BEM) approach, which solves for aerodynamic forces by analyzing the change in momentum as flow in a theoretical stream-tube crosses an idealized 2D actuator-disk representation of a wind turbine rotor plane. Due to the idealized 2D approximation of the rotor plane, classic formulations of the BEM model do not account for deformations of the blades during operation. As discussed in Section 2.1, CODEF aims to capture the effects of blade warping during operation. This is why CODEF implements the Dynamic Rotor Deformation–Blade Element Momentum (DRD-BEM) model for rotor flow, which is coupled to the GTBM structural model to perform a comprehensive analysis of aeroelastic blade behavior that includes the effects of structural and mechanical misalignment of the blade sections relative to the incoming wind flow [19].

To achieve such consideration of blade section misalignment, the DRD-BEM model performs a series of coordinate transformations via orthogonal linear operators to account for relevant mechanical actions and the physical deformation of blade sections. This process begins with the incoming wind velocity, $\mathbf{W}_{\infty wind}$, and aims to eventually express this velocity in the blade section coordinate system to evaluate the total aerodynamic load at each time-step of the ODE solution.

First, $\mathbf{W}_{\infty wind}$ is transformed to align the velocity of incoming wind relative to the coordinate system of the hub, h. Adjustments to the hub orientation, such as yaw, tilt, and instantaneous angle of azimuth, are applied via linear operators $\mathbf{C}_{\Delta\theta_{yaw}}$, $\mathbf{C}_{\theta_{tlt}}$, and $\mathbf{C}_{\theta_{az}}$, respectively.

$$\mathbf{W}_{\infty h} = \left(\mathbf{C}_{\theta_{az}}\mathbf{C}_{\theta_{tlt}}\mathbf{C}_{\Delta\theta_{yaw}}\mathbf{W}_{\infty wind}\right) \tag{1}$$

An examplary linear operator for yaw-induced misalignment of the hub can be seen expressed as an orthogonal matrix, where $\Delta\theta_{yaw}$ defines the angle of yaw offset relative to $\mathbf{W}_{\infty wind}$.

$$\mathbf{C}_{\Delta\theta_{yaw}} = \begin{bmatrix} \cos(-\Delta\theta_{yaw}) & \sin(-\Delta\theta_{yaw}) & 0 \\ -\sin(-\Delta\theta_{yaw}) & \cos(-\Delta\theta_{yaw}) & 0 \\ 0 & 0 & 1 \end{bmatrix}, \tag{2}$$

Once in the coordinate system of the hub, effects from interference at the rotor can be introduced using the axial and tangential induction factors, a and a'.

$$\mathbf{W}_h = \begin{bmatrix} W_{\infty h_x}(1-a) \\ W_{\infty h_y} + \Omega\, r_h a' \\ W_{\infty h_z} \end{bmatrix} \tag{3}$$

Next, $\mathbf{W}_h$ is transformed to the coordinate system of the blade root, b, to account for misalignment due to coning and pitch, using linear operators $\mathbf{C}_{\theta_{cn}}$ and $\mathbf{C}_{\theta_p}$, respectively. Next, $\mathbf{C}_{Lb}$ transforms blade-root coordinates into undeformed blade-section coordinates, along reference line L. Finally, to reach the deformed blade-section coordinate system, l, linear operator $\mathbf{C}_{lL}$ is employed to reflect time-dependent solutions of blade warping from the structural model. At this time, velocity components $\mathbf{v}_{str}$ and $\mathbf{v}_{mech}$ can also be added to account for associated structural vibrations and mechanical actions, respectively.

$$\mathbf{W}_l = \left(\mathbf{C}_{lL}\mathbf{C}_{Lb}\mathbf{C}_{\theta_p}\mathbf{C}_{\theta_{cn}}\mathbf{W}_h\right) + \mathbf{v}_{str} + \mathbf{v}_{mech} \tag{4}$$

Calculations of each blade section's total aerodynamic load can be evaluated using lift, drag, and moment coefficients associated with the relative angle of attack of the incoming inflow velocity. After forces of drag and lift are distributed appropriately into the airfoil's chord-wise and chord-normal directions, a series of backwards transformations can be computed using the transpose of the aforementioned linear operators to project the total dynamic load back into the coordinate system of the hub.

2.3. Farm-Flow Model

In this work, an investigation of wind farm fluid flow is performed to evaluate the effects of alterations to blade structure and flexibility. To perform this accurately, we must use a high-fidelity model for aerodynamic fluid–structure interactions which is capable of capturing effects at a multi-turbine scale. To model these flow dynamics at a moderate cost of computation, CODEF uses a novel technique called the Gaussain-Core Vortex-Lattice Model (GVLM).

Introduced in Baruah and Ponta [23], the GVLM operates in cooperation with the DRD-BEM model to calculate the circulation of flow around sections of the blade and project the advection of vortex-wake structures downstream of the turbine. Later in this paper, we use these vortex-lattice structures to analyze wind farm inter-turbine wake interactions and the induction of velocity patterns at downstream locations of fluid flow.

In this section, a brief description of the GVLM and the role it plays on the present work is presented in order to make this paper self-contained. For a complete description of the GVLM theoretical basis and its insertion into the CODEF suite, the reader is referred to Baruah and Ponta [23], which also includes a complete derivation of its mathematical formulation and a description of the sequential procedure for the generation of the GVLM's vortex-lattice structures.

Baruah and Ponta [23] also include a series of validation tests, which compare wind-turbine wake velocity patterns from LiDAR field measurements conducted at SNL's SWiFT facility and reported by Herges et al. [24], with the corresponding results obtained from the GVLM simulations.

As discussed in Section 2.2, the DRD-BEM produces solutions of instantaneous inflow wind velocity relative to the aerodynamic attitude of warped blade sections. These DRD-BEM solutions provide the GVLM of the flow circulation characteristics necessary to create a representative bound vortex filament for each blade section element using the Kutta–Jukowski Theorem. These vortex filaments are generated for all span-wise blade sections, at time-steps of the ODE solution, to form an interconnected vortex-filament lattice structure that describes the turbine's vortex-wake dynamics [25].

As this vortex-lattice structure is advected downstream of the turbine, it evolves due to interactions with the background atmospheric flow in addition to the influence of other turbines and turbine wakes within the wind farm. The analyses presented in this work use the GVLM solutions of vortex-wake structure interactions to project depictions of farm flow velocity patterns in the simulated wind farm layout. In the CODEF-GVLM, this induced velocity can be calculated from the vortex filament structure at any desired point within a domain of fluid flow using a custom application of the Biot–Savart Law described in Ponta et al. [26].

In contrast to the Biot–Savart Law singularity representation of vorticity, the core of vortex filaments used in the CODEF-GVLM exhibit a Gaussian distribution. This is performed to emulate more realistic viscous decay, compared to the singularity approach, which does not model any dissipation of the vortex core [27]. The Gaussian-core approach is also more computationally advantageous due to the reduction in memory required, as sufficiently dissipated vortex filaments are removed from computations. Additionally, the Gaussian distribution of vortex-filament cores prevents an issue with singularity-concentrated vortex filaments, where unrealistically high projections of tangential velocity occur at radial locations near to the vortex-filament core. Avoiding this overestimation

ensures a more accurate definition of vortex-filament velocity induction at close radial proximity to the filament core.

For further discussions regarding vortex-lattice methods, and velocity-induction patterns by vortex filaments, the reader is referred to Ponta and Jacovkis [26], Strickland et al. [28], Cottet and Koumoutsakos [29], and Karamcheti [30]. For details about the Gaussian-core vortex theory and the process of formation and shedding vortex cores, the reader is referred to Ponta [27], Lamb [31], Batchelor [25], Trieling et al. [32], Flór and van Heijst [33], and Hooker [34].

In terms of how the GVLM represents the influence of incident-wind velocity profiles, given by vertical sheer exponent, veer, wind direction, and yaw offset, the reader is refereed to Baruah and Ponta [23], which also describes how turbulent fluctuations in the atmospheric flow are included in the model. In particular, Section 3.2 of that work includes a detailed discussion on how atmospheric turbulence effects are introduced into the CODEF-GVLM model via the definition of a Turbulent Diffusivity Coefficient (TDC), which can be thought as a vortex-lattice equivalent to the modeling of sub-grid scales of turbulence represented by an 'eddy viscosity' in the context of RANS or LES codes. The value of TDC was calibrated by comparing the GVLM results with LiDAR measurements of wake velocity patterns for a series of scenarios with a different turbulence intensity.

3. Numerical Experiments and Analysis of Results

This section focuses on a series of tests designed to analyze turbine-to-turbine interactions within a farm. In our current study, we present results of the wind turbines with the innovative blades developed as a part of the National Rotor Testbed (NRT) project (see Kelley [35] for a complete description of the NRT's blade design and control systems). The two SNL-NRT turbines in our simulation follow a physical layout similar to the one at the SWiFT facility, as described in Berg et al. [36], with a streamwise separation of five rotor diameters (see Figure 1).

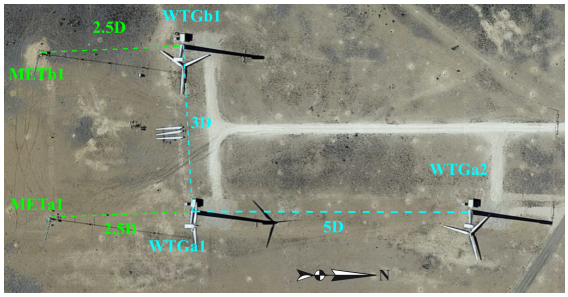

Figure 1. Satellite view of SNL's SWiFT site layout.

The SNL-SWiFT facility involves one of the most detailed field measurement campaigns of the dynamics of rotors and their wakes on a wind farm. In addition to the existing comprehensive database (see Kelley and Naughton [37,38]), obtained as part of the extensive single-turbine wake measurement campaign [24], future plans include the expansion of the facility to capture turbine-to-turbine interactions (see Barone and White [39]). The SWiFT site also supports the development and evaluation of innovative wind turbine rotor technology.

Table 1 shows the test-case matrix summarizing the four different scenarios for these twin-turbine tests. Given the extent of the twin-turbine simulation cases, the sample of wind conditions reported here is limited to the typical wind speed of 6 m/s found at the SWiFT site, with wind shear exponent Alpha corresponding to daytime and nighttime conditions. Two extra scenarios were created by adding a yaw offset of 10° to explore the effect of that parameter. The values of control system parameters like Tip Speed Ratio (TSR) and blade pitch settings for these experiments correspond to the NRT's original design settings for those wind conditions.

Table 1. Summary of typical day and night conditions at SWiFT facility used for the NRT turbine simulations.

Scenario	Wind Speed [m/s]	Alpha	TSR	Yaw Offset [deg]
NRTD1	6	0.06	9	0°
NRTD2	6	0.06	9	10°
NRTN1	6	0.30	9	0°
NRTN2	6	0.30	9	10°

These simulations were run for a period of time long enough to allow for the two vortex lattices produced by each one of the turbines to grow, overlap, and interact with each other until the twin-wake evolution reaches a statistically stable regime.

Figure 2 shows an example of how the development of the twin vortex-lattice ensemble looks at six successive instances from 30 s to 80 s for the case of the NRT's baseline blade design operating in the N1 scenario.

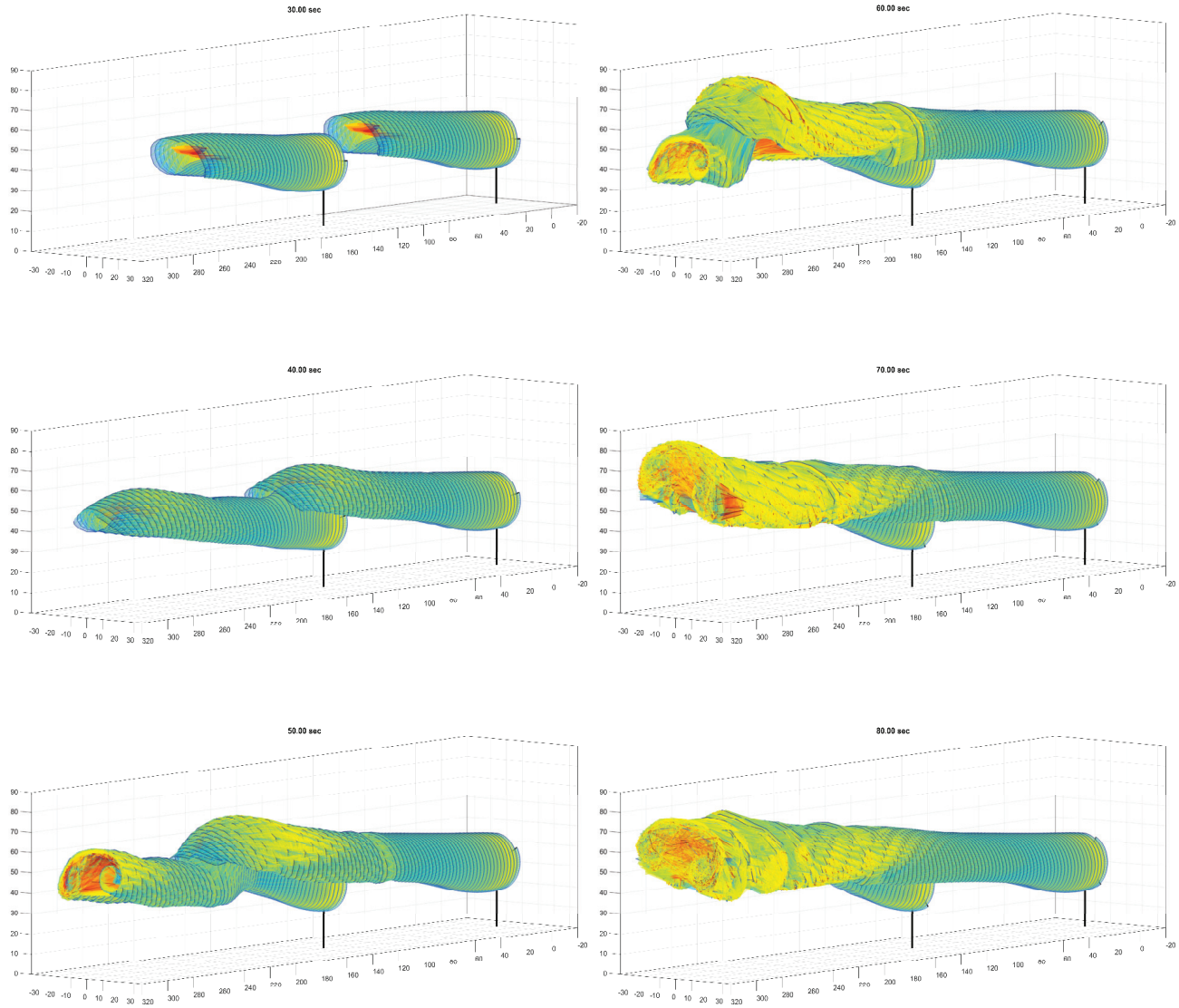

Figure 2. Example of development of the twin vortex-lattice ensemble at six successive instances, from 30 s to 80 s, for the case of the baseline blade operating in the N1 scenario. The color scheme used in all vortex lattice images is intended to provide a better appreciation of the lattice shape development and is not attached to a specific physical quantity.

3.1. Aeroelastic Response of the SNL-NRT Rotor Operating in a Waked Condition

The visualization of the vortex-lattice progression in Figure 2 is accompanied by two plots showing a selected sample of the the corresponding time evolution of blade and hub variables to illustrate the different aeroelastic response of the the upwind turbine (T1) versus the downwind one (T2).

Figure 3 shows a comparison of the blade tip deflection for the upwind and downwind turbines during the full simulation sequence, plus a close-up view of the period corresponding to the stable oscillatory regime. Figure 4 shows the corresponding time evolution for the instantaneous torque at the hub.

These plots show how, after a transitional period where the two lattices grow, overlap, and interact, the signals exhibit a stable oscillatory regime on which the magnitude of relevant operational parameters could be evaluated. In the case of these scenarios, the stable period of the oscillatory regime starts approximately around the 75 s mark (depending on the case).

Several other operational parameters of the rotor were also studied (e.g., blade twist angle at the tip, blade-root bending moment, instantaneous hub thrust, and instantaneous hub power), and all of them exhibited the same type of qualitative behavior than the blade tip deflection (Figure 3) and hub torque (Figure 4).

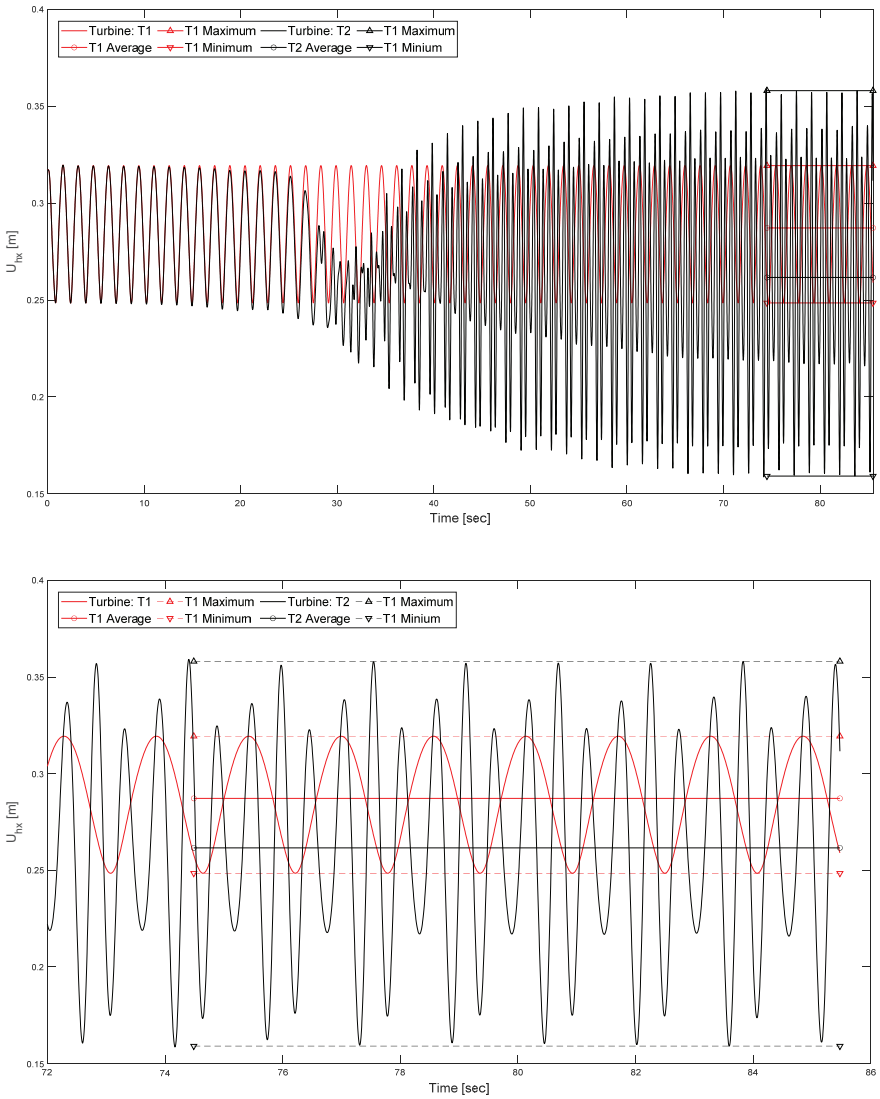

Figure 3. Time evolution of blade tip deflection of the upwind (T1) and downwind (T2) turbines for the N1 scenario. Top panel, full simulation sequence. Bottom panel, close-up view of the stable oscillatory regime.

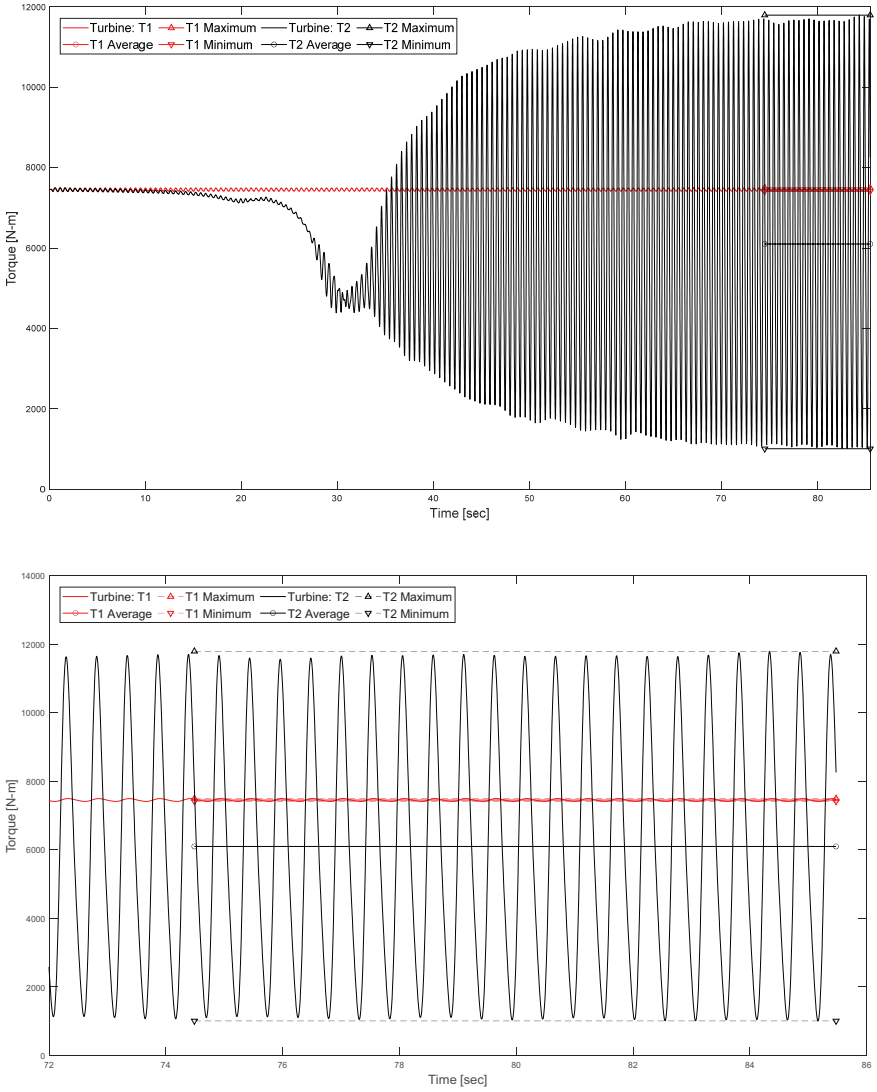

Figure 4. Time evolution of the hub torque of the upwind (T1) and downwind (T2) turbines for the N1 scenario. Top panel, full simulation sequence. Bottom panel, close-up view of the stable oscillatory regime.

3.2. Twin-Turbine Wake Characteristics of the SNL-NRT Rotor Operating in a Tandem Layout

In order to illustrate the complex series of vortex interactions that occur when the two wakes interact, the following figures will show a selection of plots that depict the wake's vortex-lattice structure and axial velocity patterns produced by the GVLM for the baseline-blade NRT rotor, operating in each of the four test-matrix scenarios listed in Table 1.

When observing the velocity pattern evolution of the diurnal cases, there are several emerging effects that can be traced back to the complex mutual advection of vortex filaments when operating within a variable background wind velocity profile, which differ substantially from the basic form exhibited by a vortex wake evolving in a steady-state uniform stream flow pattern.

To illustrate this point, Figure 5 shows an example of vortex-lattice wake generated by GVLM for the National Renewable Energy Laboratory 5 MW Reference Wind Turbine (NREL-5MW-RWT) [40], operating in a uniform-stream steady-state flow. In this simple scenario (which could be interpreted as the rotor operating in a virtual wind-tunnel flow), the lattice is generated regularly, in a manner that creates what is essentially a tubular structure corresponding to the wake core, with the bundles of filaments associated with the blade tip vortices wrapping around it in a helicoidal shape. This wake structure induces a

simple axial velocity pattern of circular contour, which essentially remains unaltered as it advects downstream, ultimately becoming weaker and dissipating due to turbulent viscous diffusion without changing its shape.

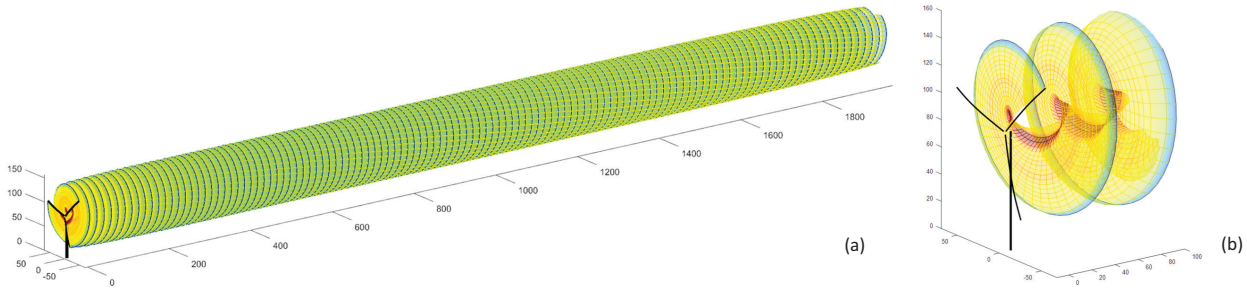

Figure 5. Example of vortex-lattice wake generated by GVLM for the NREL-5MW-RWT [40], operating in a uniform-stream steady-state flow. (**a**) Perspective of the complete wake. (**b**) Close-up of the lattice for an individual blade.

When a variable wind velocity profile is added into the simulated scenario, the regularity in the lattice generation process, previously observed in the uniform-stream background flow case, disappears. Due to the cross-flow variations in wind velocity magnitude and/or direction induced by vertical sheer exponent, veer, and yaw offset, the advection of vortex filaments located at different positions in the wake's cross-section changes their relative position, altering the tubular/helicodal shape of the basic lattice. This, in turn, induces changes in the mutual advection process of the filaments, which ultimately leads to fundamental changes in the wake-vortex structure.

As an example of this type of effect, Figure 6 shows an example of vortex-lattice wake generated by GVLM for the case of a 27 m diameter turbine, operating in a variable wind profile with a vertical shear exponent of 0.12, a veer of 1.3°, and a yaw offset of 5.9°.

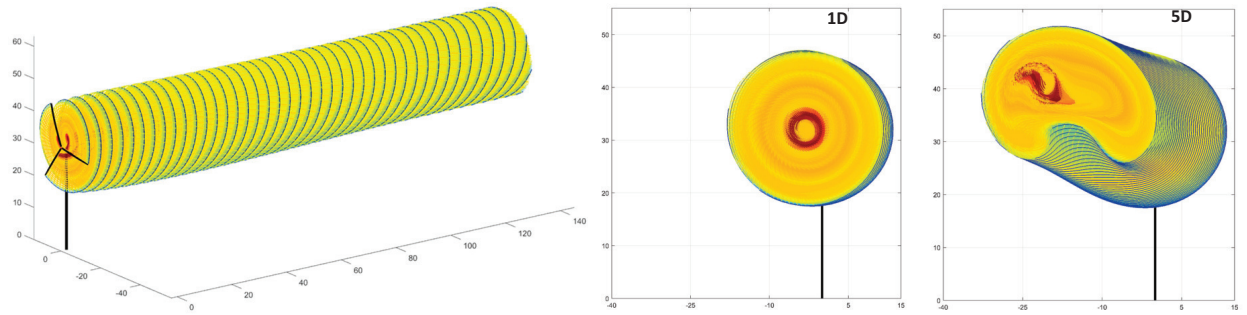

Figure 6. Example of vortex-lattice wake generated by GVLM for a 27 m diameter turbine, operating in a variable wind profile with a vertical shear exponent of 0.12, a veer of 1.3°, and a yaw offset of 5.9°, showing a perspective of the complete wake, plus rear views of the lattice cross-section at 1 and 5 turbine diameters downstream of the rotor.

Observing the the perspective of the complete wake in Figure 6, it can be seen that, even in this relatively moderate vertical sheer, the difference in advection speed makes the filaments located in the upper portions of the lattice move faster than the lower ones. This affects the relative mutual advection of vortex filaments in the vertical plane, ultimately creating what can be described as a roll-up ram-horn shape in the cross-section of the vortex structure combined with a tendency of the wake to deflect upwards as it propagates downstream, which can be clearly appreciated in the two rear views of the lattice cross-section at 1 and 5 turbine diameters downstream of the rotor, also shown in Figure 6. These, and other similar effects on the wake structure connected with the role of the incident wind velocity profile, generally referred to as wake meandering, have been observed by several

researchers (see for example Su and Bliss [41], Porté-Angel et al. [42], Abkar et al. [43], and Baruah and Ponta [23], among others).

When the wakes of two turbines located in tandem interact, the vortex evolution process becomes even more complex, generating a very rich series of secondary transitions in the vortex structure of the combined wake, which also depend on the profile of the background wind. As an example, Figure 7 shows a side-by-side comparison of the vortex-lattice structure and the corresponding wake velocity patterns for two NRT turbines operating at the conditions of the N2 matrix scenario listed in Table 1.

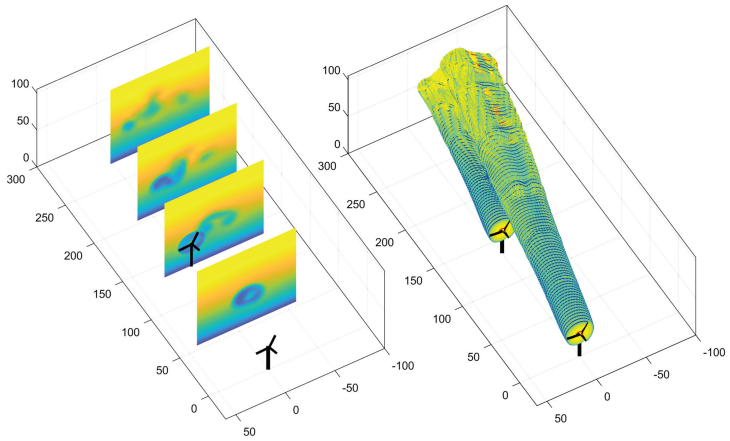

Figure 7. Example of a side-by-side comparison of the vortex lattice structure and the corresponding wake velocity patterns for two NRT turbines operating at the conditions of the N2 matrix scenario listed in Table 1.

The formation of secondary vortex structures has been observed before in the context of complex vortex streets in the wake of bluff bodies by numerous researchers, both experimentally and numerically [44–56]. In these cases, the primary vortex street becomes unstable at a certain place downstream, and the secondary vortex street is formed with patterns of vortices that differ in number, shape, and scale from the original wake shed by the body.

These secondary processes that take place in the far wake after the initial shedding and arrangement are generally triggered by changes in the body oscillatory motion or in the velocity profile of the incoming flow. Even relatively subtle changes in local velocity may induce a totally different pattern in which the wake produces separated vortex units by the splitting of a single original vortex core. This may be followed by a process of merging of neighboring vortices in close proximity, forming a set of larger vortex cores.

The extension of these notions of secondary transitions in wake-vortex structures seems to be directly applicable in the context of twin-turbine wake evolution. Here, the interaction of two separate wakes, plus the presence of a cross-sectional velocity pattern in the background wind, combine to produce the required differences in the advection of vortex filaments to trigger the same type of vortex transformation phenomena.

It is on this type of twin-wake interaction observed in the simulations of the NRT project where we shall focus our attention henceforward. For the first two matrix scenarios corresponding to the diurnal wind profiles (D1 and D2), respectively, Figures 8 and 9 show semi-transparent perspective views that mark the location of the cross-sectional planes where the axial velocity patterns are plotted, immediately followed by images of the corresponding individual planes in frontal view. The cross-sectional planes were distributed along the longitudinal axis of the twin-turbine array from a distance of -27 m upstream of T1, equivalent to one rotor diameter (1D), to a distance of 270 m downstream, equivalent to ten rotor diameters (10D). The planes were separated at intervals of 1D for the zone spanning the wake of T1, and their interspace was reduced to 0.25D for the zone downstream of T2, where the interactions between the two wakes exhibit a richer behavior. Two extra sectional planes were added in the immediate vicinity of each one of the rotors to emphasize the interactions with the flow before and after crossing the rotor's plane.

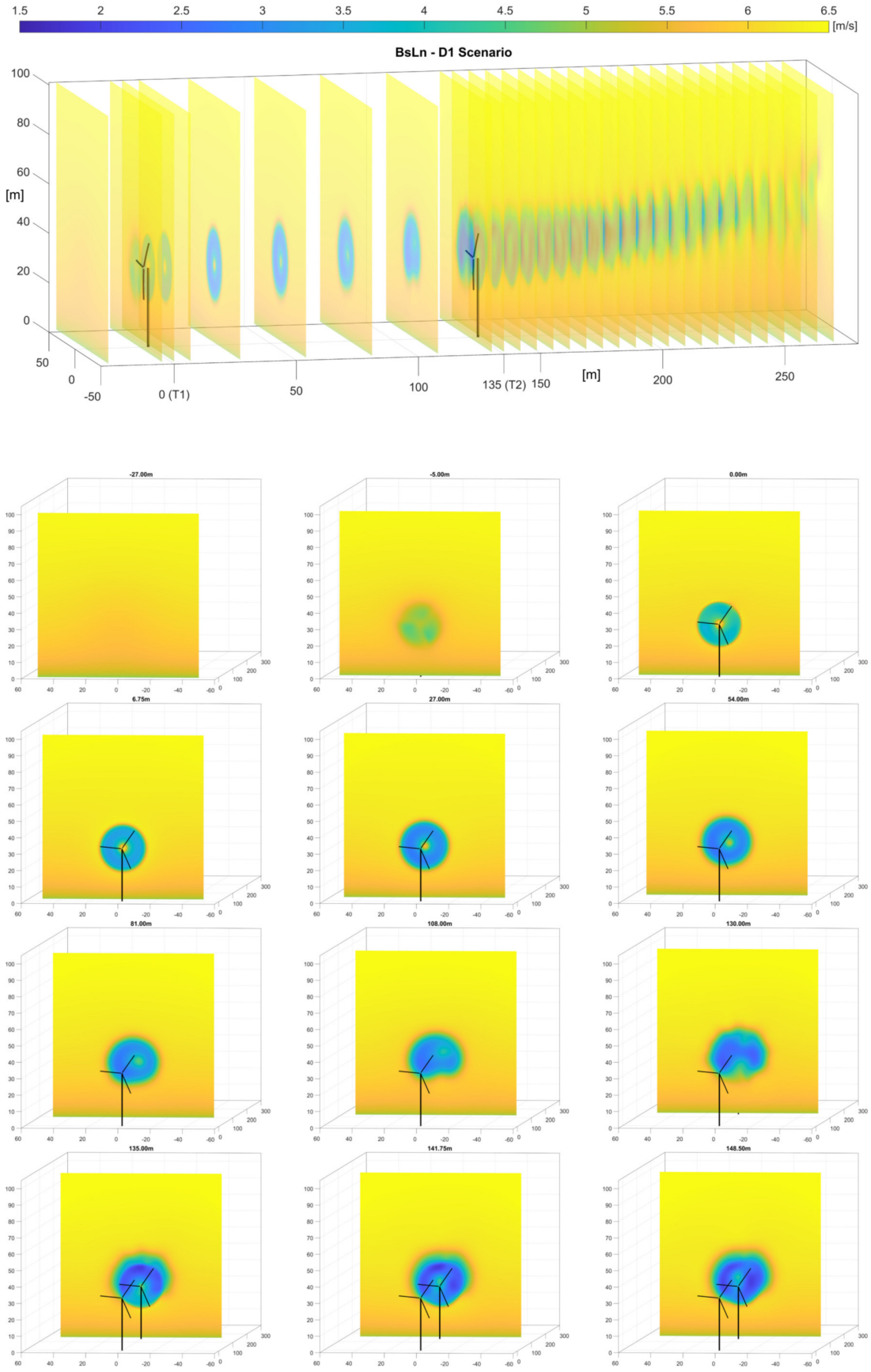

Figure 8. *Cont.*

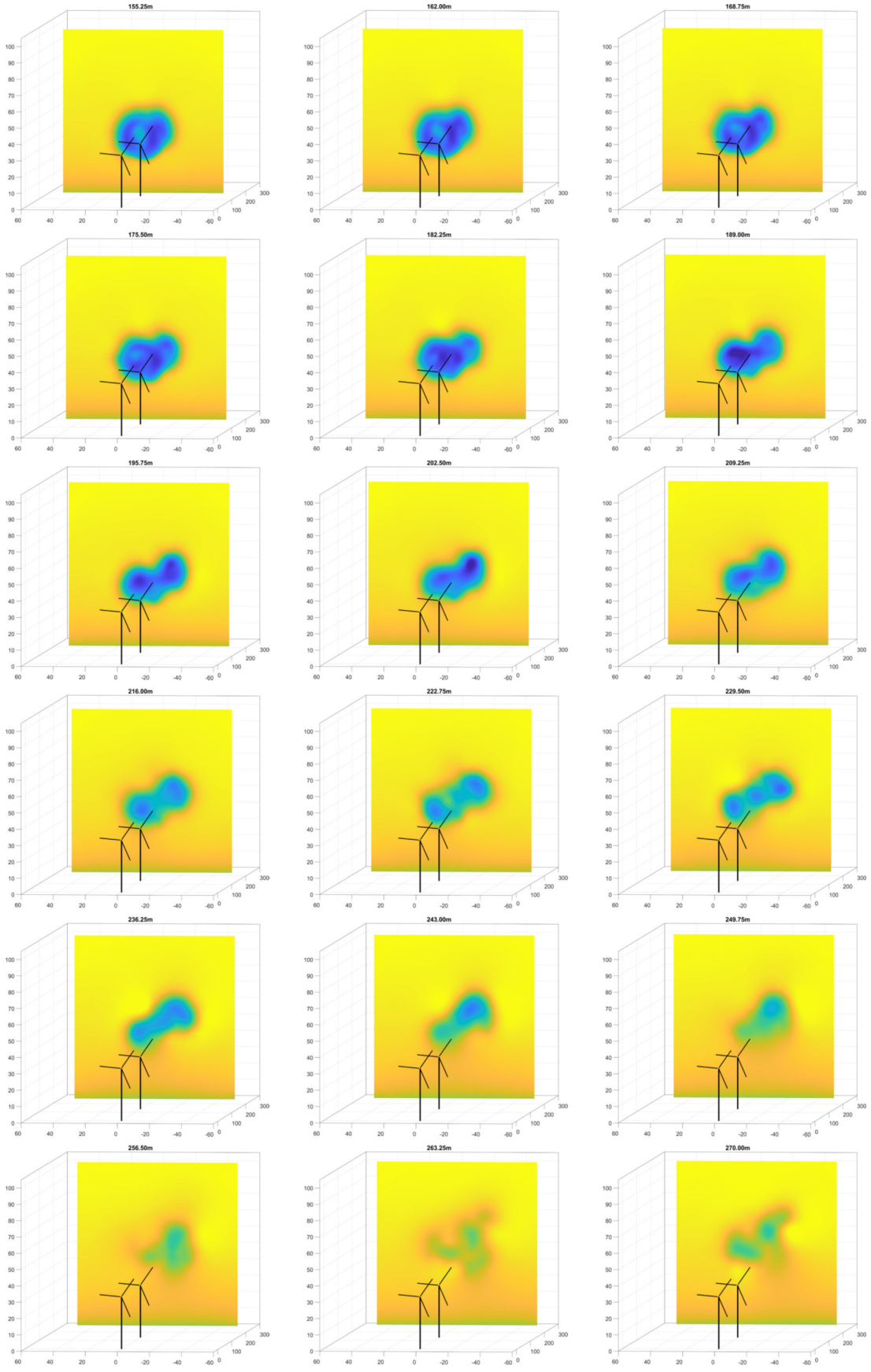

Figure 8. Semi-transparent view of the twin-wake axial velocity patterns at cross-sectional planes distributed from 1D upstream to 10D downstream of T1 for the D1 scenario followed by frontal-view images of the individual planes.

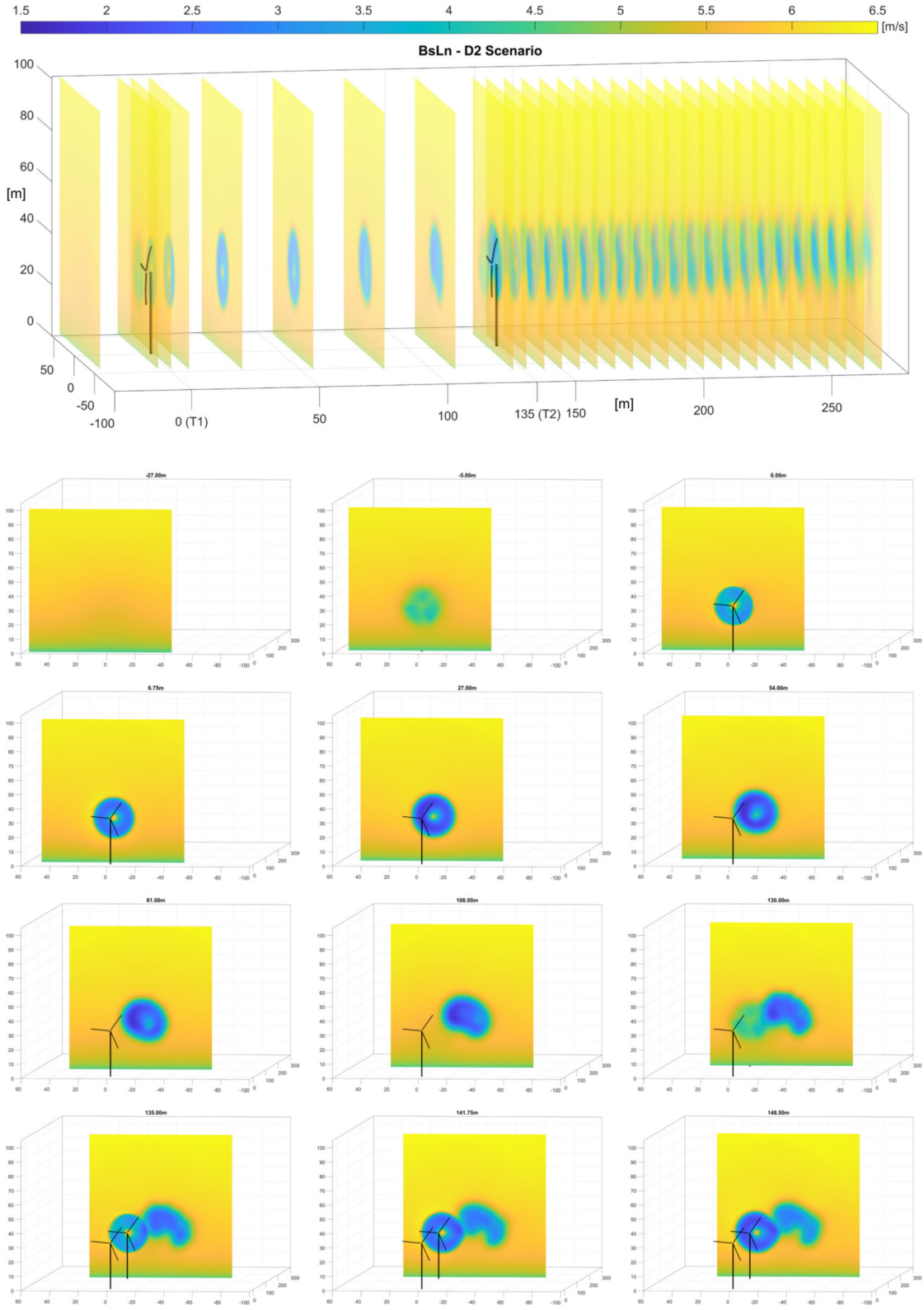

Figure 9. *Cont.*

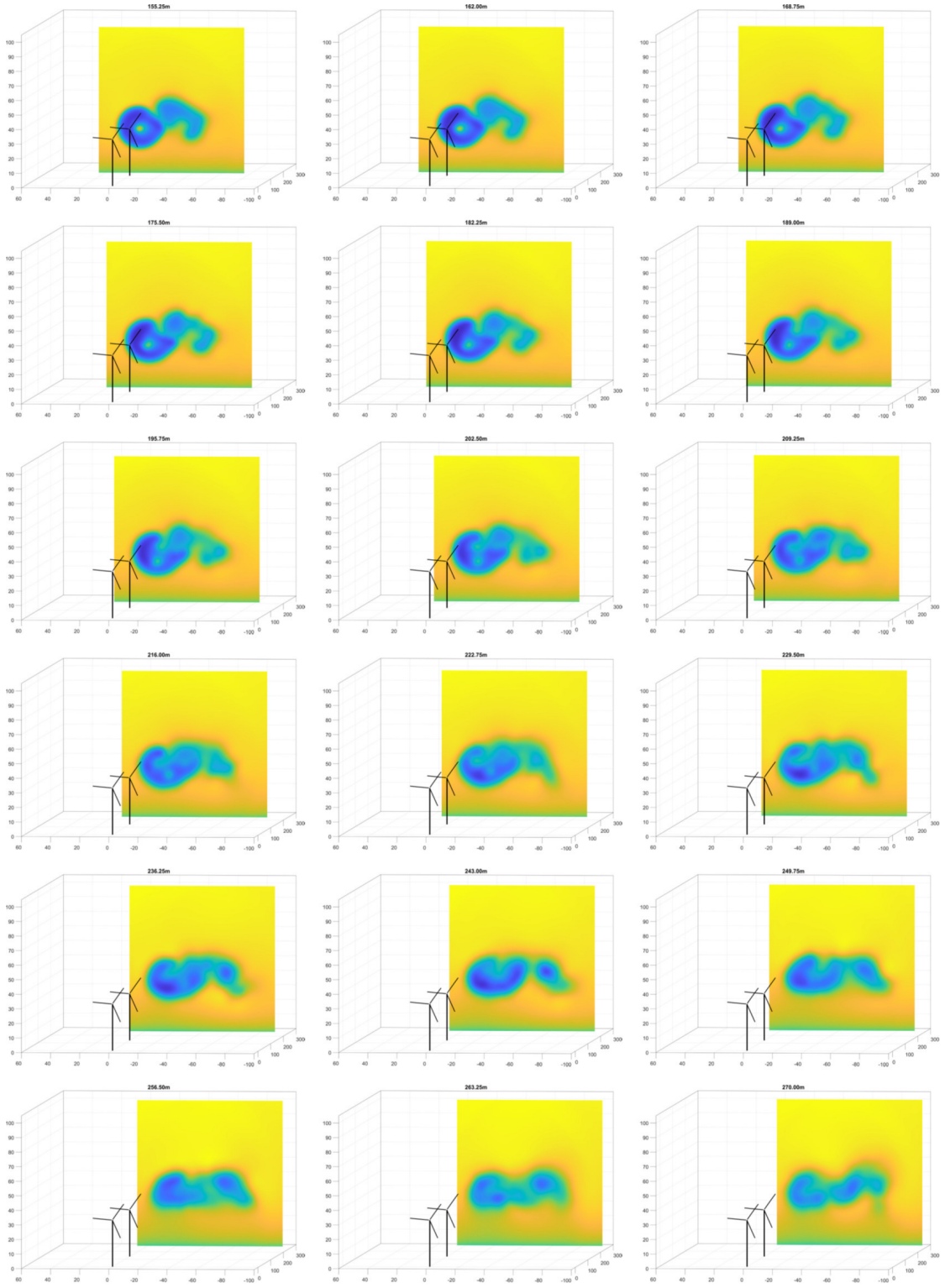

Figure 9. Semi-transparent view of the twin-wake axial velocity patterns at cross-sectional planes distributed from 1D upstream to 10D downstream of T1 for the D2 scenario followed by frontal-view images of the individual planes.

An inspection of the twin-wake evolution for the D1 scenario depicted in Figure 8 shows an example of a dual-vortex-core nucleation followed by core splitting. Even though the complete evolution could be followed in Figure 8 itself, Figure 10 identifies an excerpt of some key frames showing particular instances in the sequence of secondary transitions that serve to better illustrate the processes which are taking place. At first, when the wake

of the upwind turbine, T1, goes through the plane of the second rotor, T2, the two wakes practically overlap, with the centroid of the T1 wake slightly above the centroid of the T2 wake. This is consistent with the fact that, in the D1 scenario, the trajectory of the first wake is only slightly affected by the moderate shear of the incident wind (Alpha = 0.06) and the absence of yaw offset. Then, the two wakes become closely intermingled to induce the generation of the dual-vortex core that could be seen already formed in the central panel of Figure 10. This is followed by a triple vortex pattern created by the partial splitting of each of the cores in the dual structure that merge in the center to crate a third vortex core.

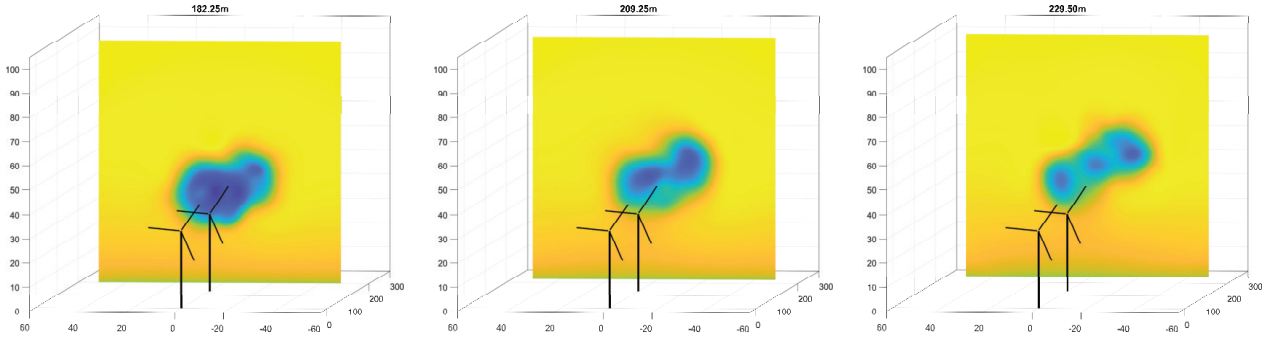

Figure 10. An excerpt of some key frames from the velocity patters in Figure 8, showing particular instances in the sequence of secondary transitions taking place in the twin-wake interaction occurring during the D1 scenario.

A similar analysis can be conducted with the inspection of Figure 9 corresponding to the D2 scenario. As before, Figure 11 identifies an excerpt of some key frames from Figure 9. In this case, due to the presence of a 10° yaw offset, the wake of T1 passes slightly above and to the side of the T2 wake. Then, a series of new vortex-core structures emerge in the space between the two wakes with a succession of core splitting and merging processes, with up to six vortex nuclei at some points, which ends in a quadruple vortex pattern spreading horizontally well to the side of the main axis of the twin-rotor array.

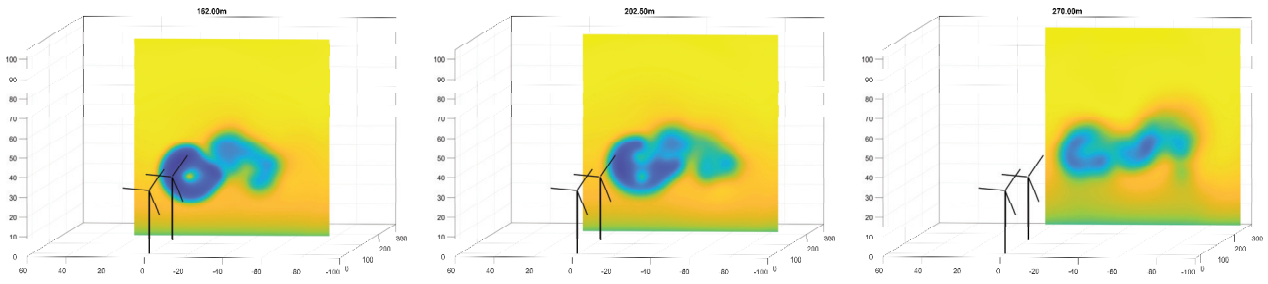

Figure 11. An excerpt of some key frames from the velocity patters in Figure 9, showing particular instances in the twin-wake interaction occurring during the D2 scenario.

For the last two matrix scenarios corresponding to the nocturnal wind profiles (N1 and N2), respectively, Figures 12 and 13 show, as it was performed before for the case of the diurnal wind profile scenarios, semi-transparent perspective views that mark the location of the cross-sectional planes where the axial velocity patterns are plotted, immediately followed by images of the corresponding individual planes in frontal view.

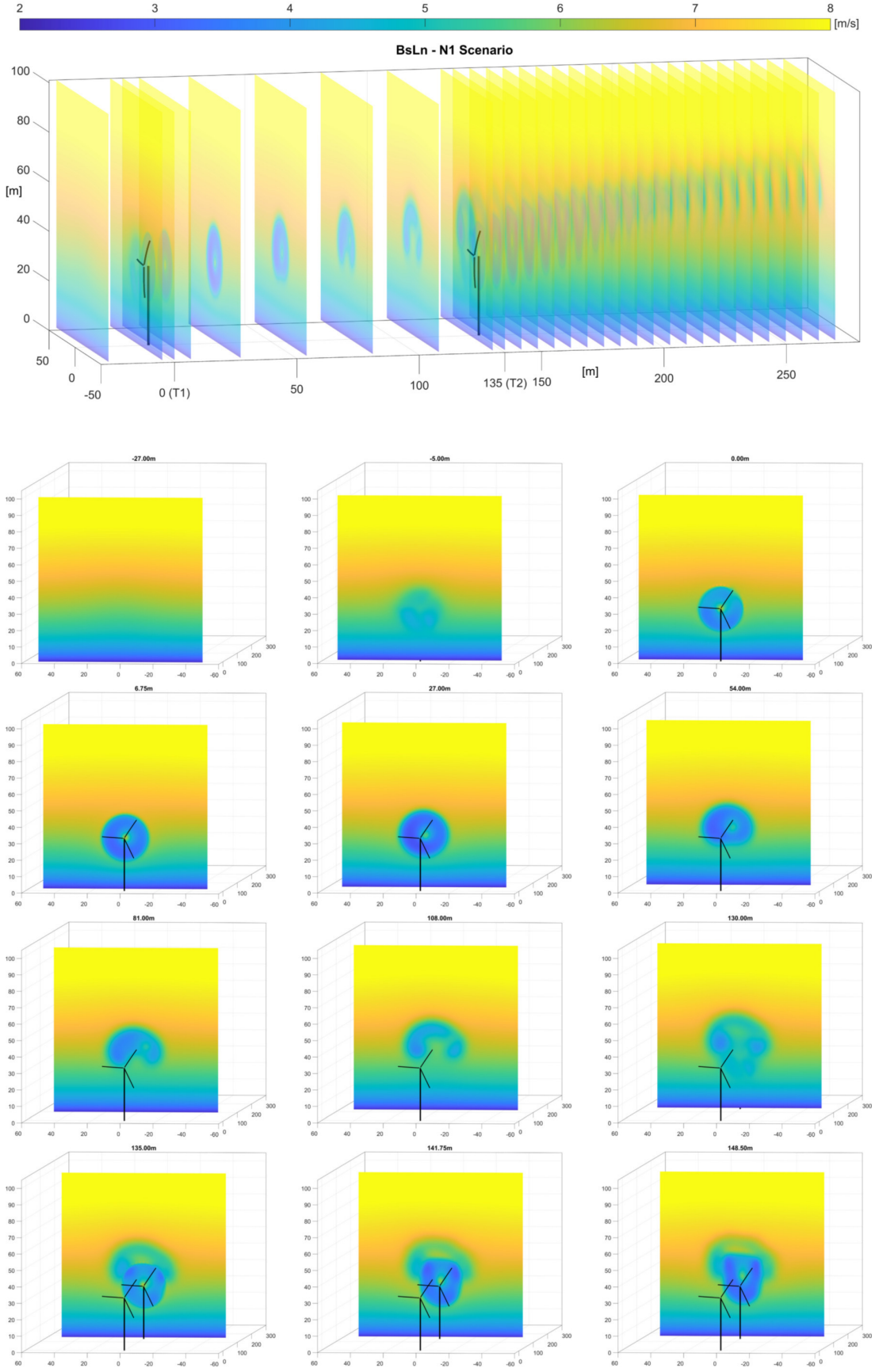

Figure 12. *Cont*.

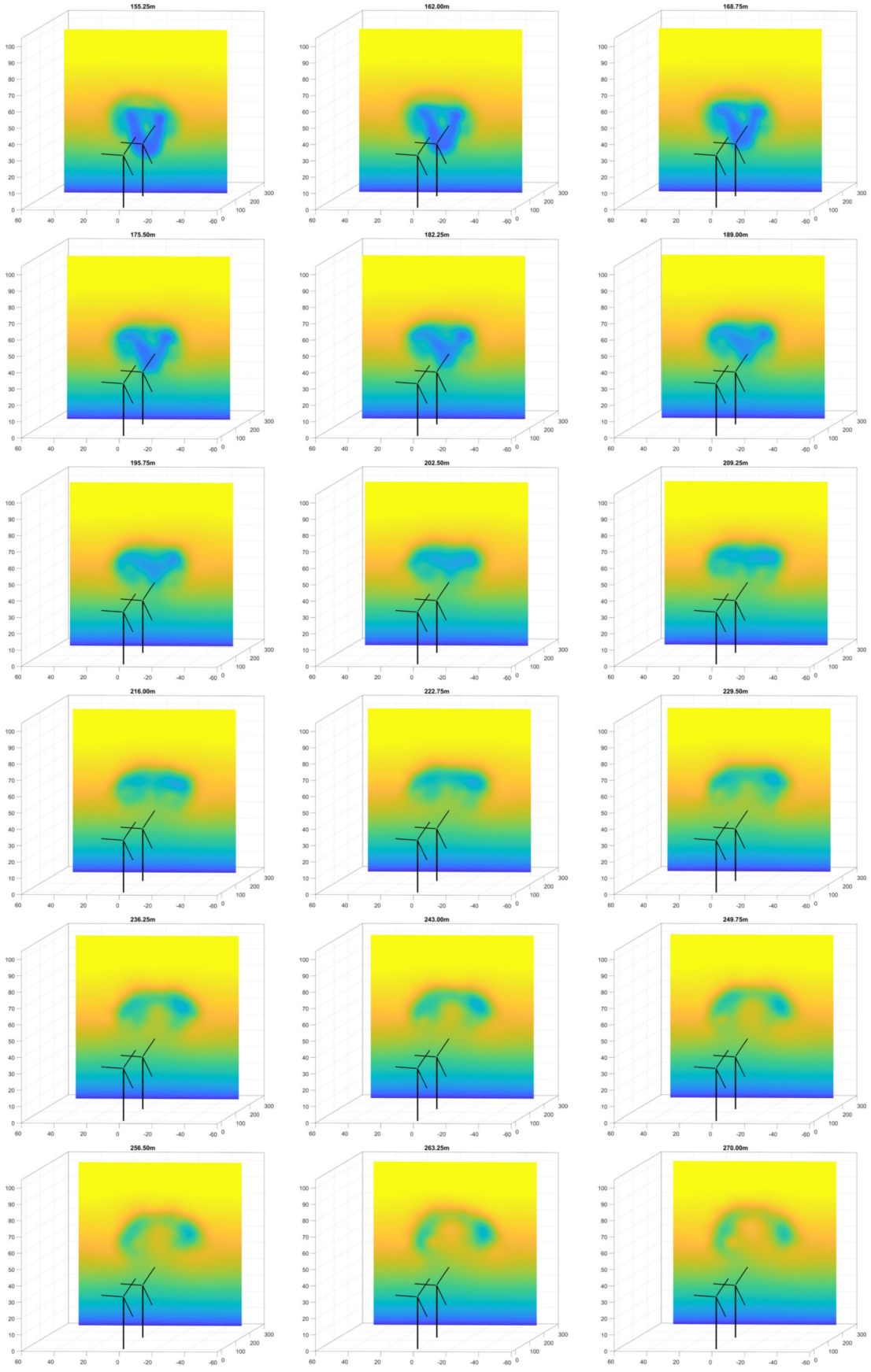

Figure 12. Semi-transparent view of the twin-wake axial velocity patterns at cross-sectional planes distributed from 1D upstream to 10D downstream of T1 for the N1 scenario followed by frontal-view images of the individual planes.

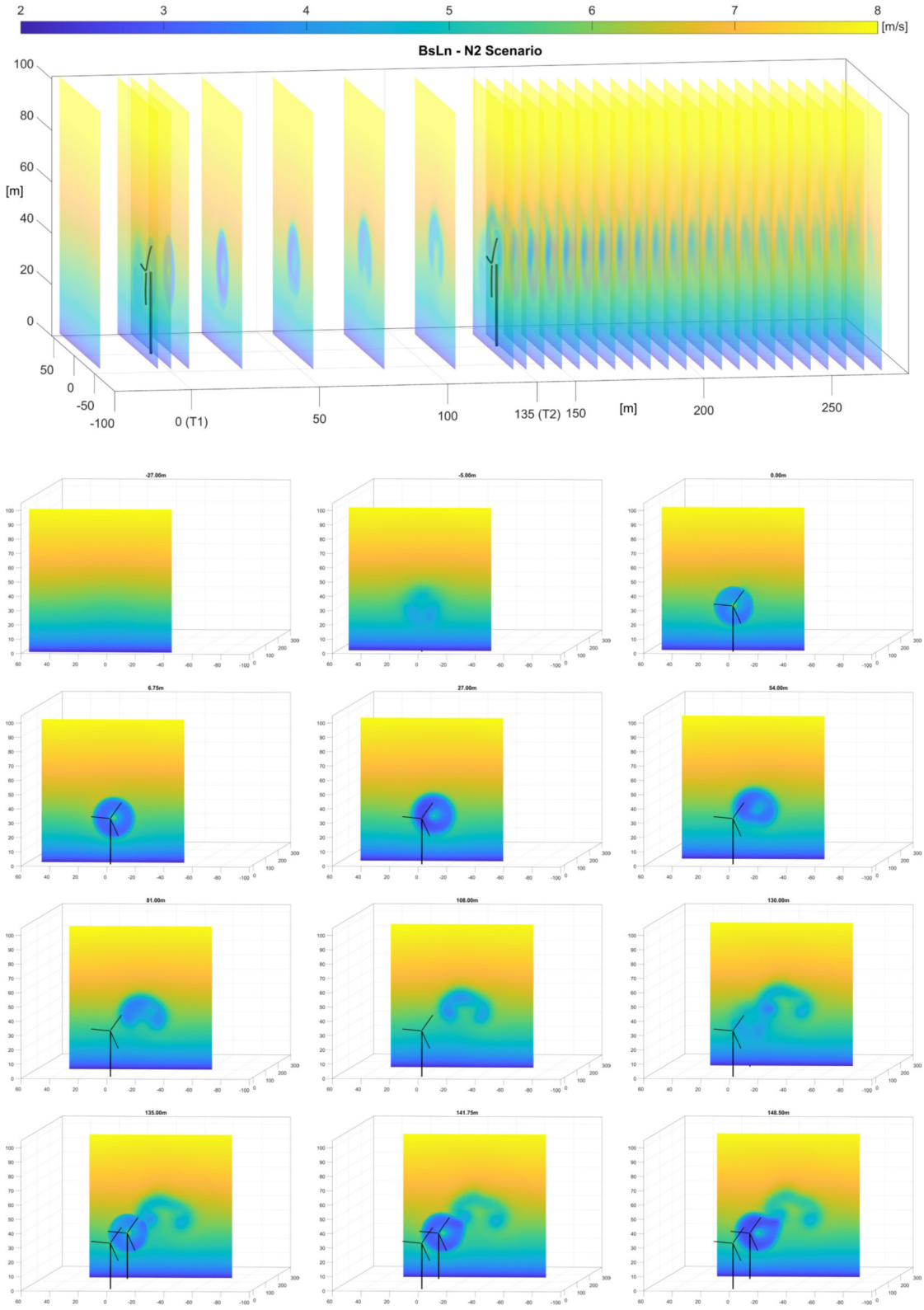

Figure 13. *Cont.*

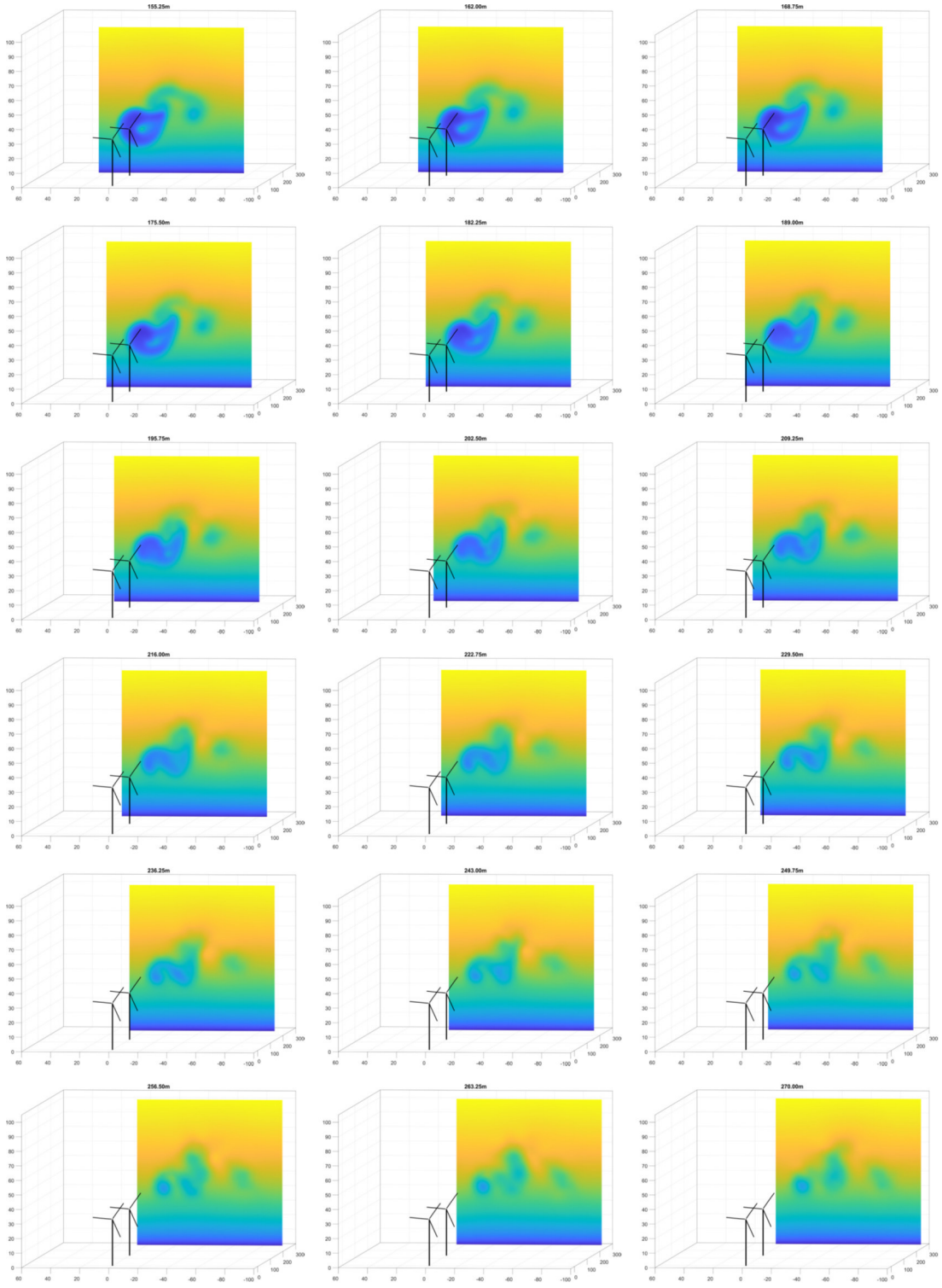

Figure 13. Semi-transparent view of the twin-wake axial velocity patterns at cross-sectional planes distributed from 1D upstream to 10D downstream of T1 for the N2 scenario followed by frontal-view images of the individual planes.

As it was performed before for the case of the diurnal wind profile scenarios, a detailed analysis can be conducted by the inspection of Figures 12 and 13 corresponding to the nocturnal wind pattern scenarios. Starting with N1, Figure 14 identifies an excerpt of some key frames from Figure 12, showing a process of absorption of the T2 wake into the remnants of the T1 wake passing over to form a mushroom-shaped structure of a stronger

nature due to the addition of the vorticity concentration of both wakes. This ultimately forms two higher concentrations of velocity-deficit spots, each one corresponding to a high concentration of vorticity. These large vorticity concentrations produced by the coalescence of vorticity content from T1 and T2 are likely to propagate farther downstream before dissipating and may have long-lasting effects on the performance of any eventual turbine located in the third row downstream of T2.

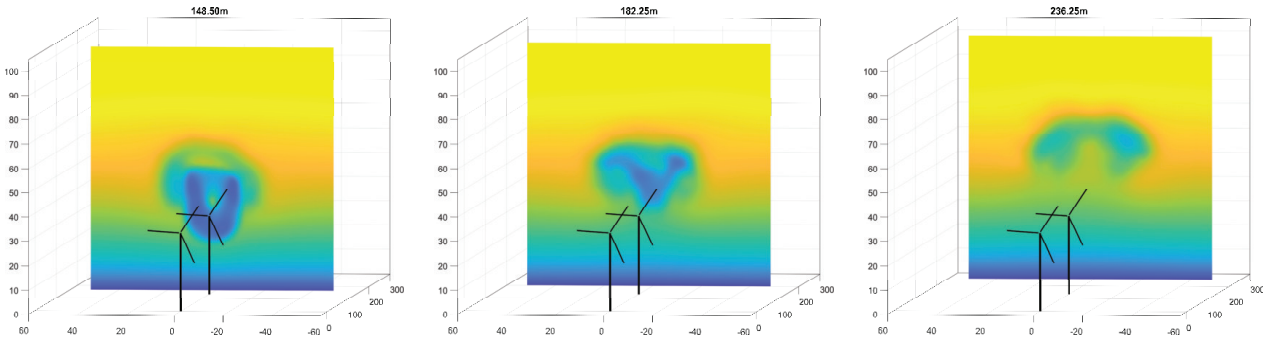

Figure 14. An excerpt of some key frames from the velocity patters in Figure 12, showing particular instances in the twin-wake interaction occurring during the N1 scenario.

Finally, Figure 15 identifies an excerpt of some key frames from Figure 13 for the N2 scenario. Due to the higher complexity of the N2 scenario in terms of the combination of high shear and yaw offset, a sequence of three secondary transitions occurs. It starts with the absorption of the T2 wake into the remnants of the T1 wake passing over and to the side, with the T1 wake already exhibiting a ram-horn shape due to the high wind shear of the nocturnal wind pattern. This creates a suction effect in a diagonal direction, followed by the splitting of the T2 wake and the 'satelization' and merging of the two central structures into a single vortex core, which leads to the final three-core pattern observed extending well to the side.

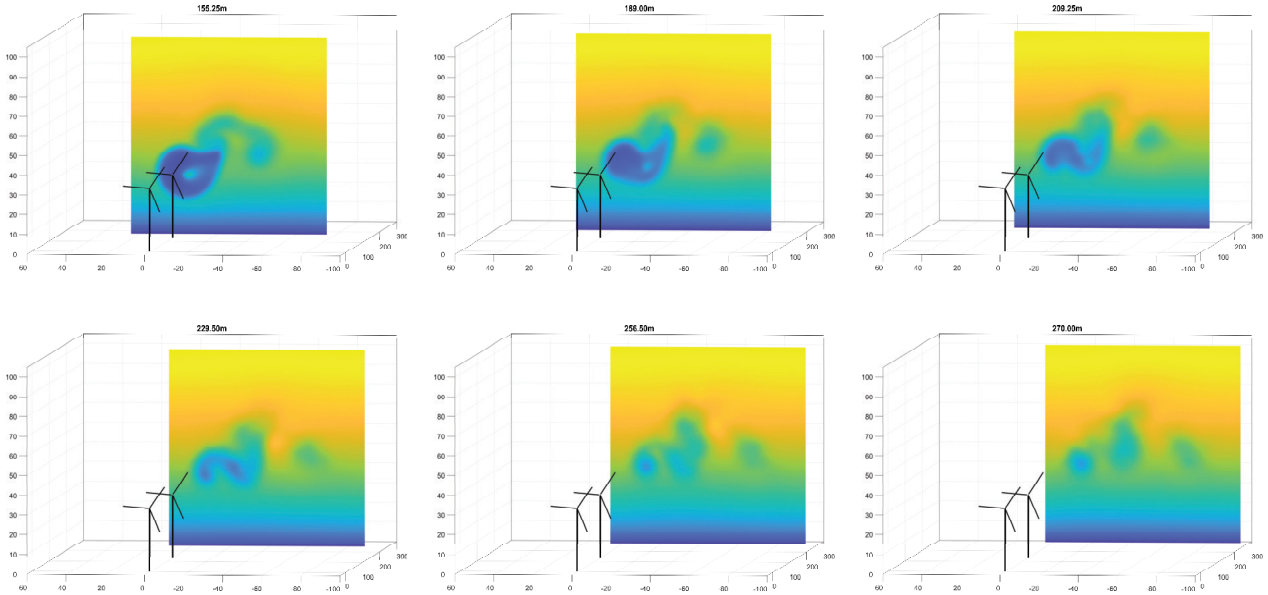

Figure 15. An excerpt of some key frames from the velocity patters in Figure 13, showing particular instances in the twin-wake interaction occurring during the N2 scenario.

4. Conclusions

In this article, several aspects of the NRT turbine's dynamic response when operating in a waked condition of a twin-turbine tandem layout were tested and reported for the

most typical wind speed registered at SNL's SWiFT facility. The aeroelastic response of the NRT baseline blade for a sample of daytime and nighttime atmospheric conditions, shown in Section 3.1, indicates the substantial influence of the upwind turbine wake on the blade's oscillatory dynamics of the downwind rotor.

The results reported in Section 3.2 serve to elucidate essential elements illustrating the complexity of vortex interactions between wakes of the upwind and downwind turbines in the tandem rotor configuration. The initial vortex pattern shed by an isolated turbine interacting with the background wind creates secondary vortex structures that affect the locus and further evolution of the zones of velocity deficit in the far wake. This fact, which is observed in all four cases listed in Table 1, confirms the fundamental importance of secondary and tertiary vortex interactions in determining wake cross-sectional shape and wake meandering.

The velocity patterns evaluated at successive cross-sectional planes presented in Figures 8–13 show several stages of vortex evolution with a richness of topological changes. In particular, when the wakes of the two turbines overlap and interact under the influence of different background-wind scenarios, a sequence of processes involving vortex stretching, splitting, and merging combine to create new wake topologies where the zones of velocity deficit can migrate, concentrate, or dissipate in complex patterns. This could be difficult to predict a priori and can certainly affect the performance of waked downwind turbines on a farm in an unexpected manner. Vortex merging represents a special challenge in terms of turbine-to-turbine interference as the new (and larger) vortical structures produced tend to survive longer and propagate farther downstream than the original vortices that compose them.

The plots shown in Figures 8–13 also serve to illustrate the effect that the different concentrations of zones of velocity deficit, created by these vortex interactions, have in the overall content of momentum and kinetic energy at several locations along the wake. These changes in the wake's axial velocity patterns alter the position, number, intensity, and shape of localized velocity-deficit zones in the wake's cross-section. As it was mentioned before, these have the capacity to substantially affect the performance and accumulated fatigue damage of eventual turbines located in subsequent rows downstream in the farm.

Regarding the latter aspect mentioned, in recent years there has been substantial research work focused on using rotor yaw as a mechanism to deflect the wake of an upwind turbine to the side of a rotor located downwind in order to avoid or minimize interference between the two turbines. The ultimate objective is to improve the performance of the downwind turbine at the expense of moderately sacrificing the performance of the upwind one in such a manner that, in the balance, the collective performance of the whole turbine array increases. One of the interesting conclusions of the present work is that, given a certain set of conditions which are not untypical in wind farm operation, the interaction of two wakes may generate an unintended reinforcement of the vorticity content of the final wake structure via the localized coalescence of part of the vorticity content of the original wakes. That means that, even tough controlled yawing is still a viable mechanism to diminish the effects of wake interaction that are detrimental to the performance of a second turbine, special care should be taken when designing a control strategy for the farm collective in order to avoid disrupting the performance of a third row of turbines by those reinforced vortical structures.

As an outlook for further work, we may observe that an extension of the tests performed here to larger farms with a greater number of turbines is worth exploring in the future. The richness of the vortex interactions observed in the wake plots of the twin-turbine layout tests presented is likely to further increase when more turbines are added to the simulated farm layout. Particularly, when more rows of turbines were added in depth, the likelihood of complex multi-wake vortex interactions emerging would increase substantially. These tests will be facilitated by the last version of CODEF, which has been expanded into a parallel evolution of the code that could be run in multi-core computers. This has enabled the model to simulate bigger farms of up to 20 turbines in its current state (keeping the same levels of fidelity and computational cost), with a potential expansion up to 80 turbines in the foreseeable future.

Author Contributions: Conceptualization, A.B., A.F. and F.P.; methodology, A.B., A.F. and F.P.; software, A.B., A.F. and F.P.; validation, A.B., A.F. and F.P.; formal analysis, A.B., A.F. and F.P.; investigation, A.B., A.F. and F.P.; resources, A.B., A.F. and F.P.; data curation, A.B., A.F. and F.P.; writing—original draft preparation, A.B., A.F. and F.P.; writing—review and editing, A.B., A.F. and F.P.; visualization, A.B., A.F. and F.P.; supervision, F.P.; project administration, F.P.; funding acquisition, F.P. All authors have read and agreed to the published version of the manuscript.

Funding: The authors gratefully acknowledge the financial support of Sandia National Labs, USA, through awards PO-2074866 and PO-2159403, and the ME-EM Department at Michigan Technological University.

Data Availability Statement: Data are contained within the article.

Conflicts of Interest: The authors declare no conflicts of interest.

References

1. Dykes, K.L.; Veers, P.S.; Lantz, E.J.; Holttinen, H.; Carlson, O.; Tuohy, A.; Sempreviva, A.M.; Clifton, A.; Rodrigo, J.S.; Berry, D.S.; et al. *IEA Wind TCP: Results of IEA Wind TCP Workshop on a Grand Vision for Wind Energy Technology*; Technical Report NREL/TP-5000-72437; National Renewable Energy Laboratory: Golden, CO, USA, 2019.
2. Veers, P.; Dykes, K.; Lantz, E.; Barth, S.; Bottasso, C.L.; Carlson, O.; Clifton, A.; Green, J.; Green, P.; Holttinen, H.; et al. Grand challenges in the science of wind energy. *Science* **2019**, *366*, eaau2027. [CrossRef]
3. Meneveau, C. Big wind power: Seven questions for turbulence research. *J. Turbul.* **2019**, *20*, 2–20. [CrossRef]
4. IEC. *Wind Turbine Generator Systems—Part 1: Design Requirements*; Technical Report IEC 61400-1:2019; International Electrotechnical Commission (IEC): Geneva, Switzerland, 2019.
5. Gebraad, P.M.; Teeuwisse, F.W.; Van Wingerden, J.; Fleming, P.A.; Ruben, S.D.; Marden, J.R.; Pao, L.Y. Wind plant power optimization through yaw control using a parametric model for wake effects—A CFD simulation study. *Wind Energy* **2016**, *19*, 95–114. [CrossRef]
6. Ekaterinaris, J.A. Numerical simulation of incompressible two-blade rotor flowfields. *J. Propuls. Power* **1998**, *14*, 367–374. [CrossRef]
7. Duque, E.; Van Dam, C.; Hughes, S. Navier-Stokes simulations of the NREL combined experiment phase II rotor. In Proceedings of the 37th Aerospace Sciences Meeting and Exhibit, Reno, NV, USA, 11–14 January 1999; p. 37.
8. Sorensen, N. Aerodynamic predictions for the unsteady aerodynamics experiment phase-II rotor at the National Renewable Energy Laboratory. In Proceedings of the 2000 ASME Wind Energy Symposium, Reno, NV, USA, 10–13 January 2000; p. 37.
9. Hansen, M.; Sorensen, J.; Michelsen, J.; Sorensen, N.; Hansen, M.; Sorensen, J.; Michelsen, J.; Sorensen, N. A global Navier-Stokes rotor prediction model. In Proceedings of the 35th Aerospace Sciences Meeting and Exhibit, Reno, NV, USA, 6–9 January 1997; p. 970.
10. Maronga, B.; Gryschka, M.; Heinze, R.; Hoffmann, F.; Kanani-Sühring, F.; Keck, M.; Ketelsen, K.; Letzel, M.O.; Sühring, M.; Raasch, S. The Parallelized Large-Eddy Simulation Model (PALM) version 4.0 for atmospheric and oceanic flows: Model formulation, recent developments, and future perspectives. *Geosci. Model Dev.* **2015**, *8*, 2515–2551. [CrossRef]
11. Churchfield, M.; Lee, S.; Moriarty, P.; Martinez, L.; Leonardi, S.; Vijayakumar, G.; Brasseur, J. A large-eddy simulation of wind-plant aerodynamics. In Proceedings of the 50th AIAA Aerospace Sciences Meeting including the New Horizons Forum and Aerospace Exposition, Nashville, TN, USA, 9–12 January 2012; p. 537.
12. Domino, S. *Sierra Low Mach Module: Nalu Theory Manual 1.0*; Sandia National Laboratories: Albuquerque NM, USA, 2015.
13. Sprague, M.A.; Ananthan, S.; Vijayakumar, G.; Robinson, M. ExaWind: A multifidelity modeling and simulation environment for wind energy. *J. Phys. Conf. Ser.* **2020**, *1452*, 012071. [CrossRef]
14. Van Bussel, G.J. The Aerodynamics of Horizontal Axis Wind Turbine Rotors Explored with Asymptotic Expansion Methods. Ph.D. Thesis, Delft University of Technology, Delft, The Netherlands, 1995.
15. Doubrawa, P.; Quon, E.W.; Martinez-Tossas, L.A.; Shaler, K.; Debnath, M.; Hamilton, N.; Herges, T.G.; Maniaci, D.; Kelley, C.L.; Hsieh, A.S.; et al. Multimodel validation of single wakes in neutral and stratified atmospheric conditions. *Wind Energy* **2020**, *23*, 2027–2055. [CrossRef]
16. Lignarolo, L.E.; Mehta, D.; Stevens, R.J.; Yilmaz, A.E.; van Kuik, G.; Andersen, S.J.; Meneveau, C.; Ferreira, C.J.; Ragni, D.; Meyers, J.; et al. Validation of four LES and a vortex model against stereo-PIV measurements in the near wake of an actuator disc and a wind turbine. *Renew. Energy* **2016**, *94*, 510–523. [CrossRef]
17. Manwell, J.F.; McGowan, J.G.; Rogers, A.L. *Wind Energy Explained: Theory, Design and Application*; Wiley: Chichester, UK, 2009.
18. Burton, T.; Sharpe, D.; Jenkins, N.; Bossanyi, E. *Wind Energy Handbook*; Wiley: Chichester, UK, 2001.
19. Ponta, F.L.; Otero, A.D.; Lago, L.I.; Rajan, A. Effects of rotor deformation in wind-turbine performance: The Dynamic Rotor Deformation Blade Element Momentum model (DRD–BEM). *Renew. Energy* **2016**, *92*, 157–170. [CrossRef]
20. Hodges, D.H. *Nonlinear Composite Beam Theory*; AIAA: Reston, VA, USA, 2006.
21. Yu, W.; Hodges, D.H.; Volovoi, V.; Cesnik, C.E.S. On Timoshenko-like modeling of initially curved and twisted composite beams. *Int. J. Sol. Struct.* **2002**, *39*, 5101–5121. [CrossRef]

22. Otero, A.D.; Ponta, F.L. Structural Analysis of Wind-Turbine Blades by a Generalized Timoshenko Beam Model. *J. Sol. Energy Eng.* **2010**, *132*, 011015. [CrossRef]
23. Baruah, A.; Ponta, F. Analysis of Wind Turbine Wake Dynamics by a Gaussian-Core Vortex Lattice Technique. *Dynamics* **2024**, *4*, 97–118. [CrossRef]
24. Herges, T.; Maniaci, D.C.; Naughton, B.T.; Mikkelsen, T.; Sjöholm, M. High resolution wind turbine wake measurements with a scanning lidar. *J. Phys. Conf. Ser.* **2017**, *854*, 012021. [CrossRef]
25. Batchelor, G.K. *An Introduction to Fluid Dynamics*; Cambridge University Press: Cambridge, UK, 2000.
26. Ponta, F.L.; Jacovkis, P.M. A vortex model for Darrieus turbine using finite element techniques. *Renew. Energy* **2001**, *24*, 1–18. [CrossRef]
27. Ponta, F.L. Vortex decay in the Kármán eddy street. *Phys. Fluids* **2010**, *22*, 093601. [CrossRef]
28. Strickland, J.H.; Webster, B.T.; Nguyen, T. A Vortex Model of the Darrieus Turbine: An Analytical and Experimental Study. *J. Fluids Eng.* **1979**, *101*, 500–505. [CrossRef]
29. Cottet, G.H.; Koumoutsakos, P.D. *Vortex Methods: Theory and Practice*; Cambridge University Press: London, UK, 2000.
30. Karamcheti, K. *Principles of Ideal-Fluid Aerodynamics*; Wiley: New York, NY, USA, 1966.
31. Lamb, H. *Hydrodynamics*, 6th ed.; Cambridge University Press: Cambridge, UK, 1932.
32. Trieling, R.R.; van Wesenbeeck, J.M.A.; van Heijst, G.J.F. Dipolar vortices in a strain flow. *Phys. Fluids* **1998**, *10*, 144–159. [CrossRef]
33. Flór, J.B.; van Heijst, G.J.F. An experimental study of dipolar structures in a stratified fluid. *J. Fluid Mech.* **1994**, *279*, 101–133. [CrossRef]
34. Hooker, S.G. On the action of viscosity in increasing the spacing ration of a vortex street. *Proc. R. Soc. Lond.* **1936**, *154*, 67–89.
35. Kelley, C.L. *Aerodynamic Design of the National Rotor Testbed*; Technical Report SAND2015-8989; Sandia National Lab.: Albuquerque, NM, USA, 2015.
36. Berg, J.; Bryant, J.; LeBlanc, B.; Maniaci, D.C.; Naughton, B.; Paquette, J.A.; Resor, B.R.; White, J.; Kroeker, D. Scaled wind farm technology facility overview. In Proceedings of the 32nd ASME Wind Energy Symposium, National Harbor, MD, USA, 13–17 January 2014; p. 1088.
37. Kelley, C.; Naughton, B. Surface Meteorological Station—SWiFT Southwest—METa1—Reviewed Data. 2021. Available online: https://www.osti.gov/biblio/1349888 (accessed on 10 December 2023).
38. Kelley, C.; Naughton, B. Lidar—DTU SpinnerLidar—Reviewed Data. 2021. Available online: https://www.osti.gov/biblio/1349890 (accessed on 10 December 2023).
39. Barone, M.F.; White, J. *DOE/SNL-TTU Scaled wind Farm Technology Facility*; Technical Report SAND2011-6522; Sandia National Lab.: Albuquerque, NM, USA, 2011.
40. Jonkman, J.; Butterfield, S.; Musial, W.; Scott, G. *Definition of a 5-MW Reference Wind Turbine for Offshore System Development*; Technical Report NREL/TP-500-38060; National Renewable Energy Laboratory: Golden, CO, USA, 2009.
41. Su, K.; Bliss, D. A numerical study of tilt-based wake steering using a hybrid free-wake method. *Wind Energy* **2020**, *23*, 258–273. [CrossRef]
42. Porté-Agel, F.; Bastankhah, M.; Shamsoddin, S. Wind-Turbine and Wind-Farm Flows: A Review. *Bound.-Layer Meteorol.* **2020**, *174*, 1–59. [CrossRef]
43. Abkar, M.; Sørensen, J.N.; Porté-Agel, F. An Analytical Model for the Effect of Vertical Wind Veer on Wind Turbine Wakes. *Energies* **2018**, *11*, 1838. [CrossRef]
44. Ponta, F.L.; Aref, H. Numerical experiments on vortex shedding from an oscillating cylinder. *J. Fluids Struct.* **2006**, *22*, 327–344. [CrossRef]
45. Williamson, C.H.K.; Roshko, A. Vortex formation in the wake of an oscillating cylinder. *J. Fluids Struct.* **1988**, *2*, 355–381. [CrossRef]
46. Williamson, C.H.K.; Prasad, A. A new mechanism for oblique wave resonance in the natural far wake. *J. Fluid Mech.* **1993**, *256*, 269–313. [CrossRef]
47. Govardhan, R.; Williamson, C.H.K. Modes of vortex formation and frequency response of a freely vibrating cylinder. *J. Fluid Mech.* **2000**, *420*, 85–130. [CrossRef]
48. Griffin, O.M.; Ramberg, S.E. The vortex street wakes of vibrating cylinders. *J. Fluid Mech.* **1974**, *66*, 553–576. [CrossRef]
49. Meneghini, J.R.; Bearman, P.W. Numerical simulation of high amplitude oscillatory flow about a circular cylinder. *J. Fluids Struct.* **1995**, *9*, 435–455. [CrossRef]
50. Aref, H.; Siggia, E. Evolution and breakdown of a vortex street in two dimensions. *J. Fluid Mech.* **1981**, *109*, 435–463. [CrossRef]
51. Cimbala, J.M.; Nagib, H.M.; Roshko, A. Large structure in the far wakes of two-dimensional bluff bodies. *J. Fluid Mech.* **1988**, *190*, 265–298. [CrossRef]
52. Inoue, O.; Yamazaki, T. Secondary vortex streets in Two-dimensional cylinder wakes. *Fluid Dyn. Res.* **1999**, *25*, 1–18. [CrossRef]
53. Matsui, T.; Okude, M. Formation of the secondary vortex street in the wake of a circular cylinder. In Proceedings of the IUTAM Symposium on Structures of Compressible Turbulent Shear Flows, Marseille, France, 31 August–3 September 1983; Springer: Berlin/Heidelberg, Germany, 1983; pp. 156–164.
54. Meiburg, E. On the role of subharmonic perturbations in the far wake. *J. Fluid Mech.* **1987**, *177*, 83–107. [CrossRef]

55. Taneda, S. Downstream development of the wakes behind cylinders. *J. Phys. Soc. Jpn.* **1959**, *14*, 843–848. [CrossRef]
56. Ponta, F.L.; Aref, H. Vortex synchronization regions in shedding from an oscillating cylinder. *Phys. Fluids* **2005**, *17*, 011703. [CrossRef]